Contact Electrification of Suspended Particles in a Turbulent Fluid

Xing Jin and Jeffrey S. Marshall
Dept. of Mechanical Engineering
University of Vermont, Burlington
phone: (1) 802-656-3826
e-mail: jmarsha1@uvm.edu

***Abstract*— A probabilistic version of a well-known phenomenological model for contact electrification is used to examine the effect of fluid turbulence on charge development for suspended particles as a function of the particle Stokes number. The distribution of particle collisions and particle charge appear to approach asymptotic states for high values of the Kolmogorov-scale Stokes numbers, exhibiting approximately normal distributions.**

I. INTRODUCTION

Contact electrification is the transfer of charge that occurs when two particles collide with each other or when a particle collides with or rolls along a surface [1]. This phenomenon of charge transfer is usually called *contact electrification* when it occurs as a result of particle collisions and it is called *triboelectric charging* (or tribocharging) when it occurs due to frictional contact between materials that slide or roll relative to each other. Contact electrification of particulates in a turbulent flow occurs widely in both industrial and natural processes. Contact electrification in various process industries, such as coal mining, sawmills, grain mills and storage facilities, is known to lead to dangerous explosions of dust clouds [2]. Contact electrification is responsible for development of electric field gradients leading to formation of lightning in sandstorms [3-5] and volcanic eruptions [6-7]. Contact electrification due to dust storms plays a particularly important role on dusty planets, such as Mars, where it is responsible for the strong ambient charging of dust particles [8-10]. A leading theory for development of electric charge within thunderstorms is that it is caused by contact electrification due to collision of ice particles within the storm cell [11-12]. Similarly, contact electrification of ice particles in planetary ring systems, such as that of Saturn, lead to particle charging that influences the structure of the rings and their interaction with the planetary atmosphere [13-14]. A theoretical study by Desch and Cuzzi [15] propose contact electrification of micrometer-scale particles in a turbulent environment as being responsible for formation of lightning in the solar nebula, which is important for formation of the small mm-scale chondrules that serve as the building blocks of the planetary system.

There has been a great deal of recent research on fundamental issues associated with particle contact electrification. Despite its importance to a large range of problems, many fundamental aspects of contact electrification remain unresolved. Even the most basic question of what exactly is transferred between the two colliding materials that gives rise

to the charge differential is at present not entirely clear, and may in fact differ for different types of contact electrification processes. The problem is not a lack of explanations for the electrification process, but instead too many plausible explanations. Material particles, ions and electrons have all been proposed as possible charge carriers [16-20]. A traditional view of contact electrification is represented by the triboelectric series, which empirically orders materials to indicate the direction of charge transfer during contact electrification. However, the triboelectric series is not always reproducible [21-22], and order within the series can sometimes be reversed, such as following ultraviolet irradiation [23]. Contact electrification has also frequently been observed between chemically identical insulator particles [24-26]. Material inhomogeneity, asymmetric contact, electron band gap defects, and local polarization have all been used to explain the charging mechanism [19, 24, 27-29].

Despite on-going research on the fundamental physics of contact electrification, reasonable phenomenological models of particle charge exchange exist with which one might proceed to investigate other issues associated with the phenomenon [25, 30-32]. Following this line of thought, the current paper examines the influence of the surrounding turbulent flow field on the particle electrification process. We note that contact electrification examples, such as those discussed in the first paragraph of this section, take place in a wide variety of fluid flow environments, ranging from normal earth atmosphere to the low-pressure Martian atmosphere to the near-vacuum conditions of Saturn's rings, and for particle sizes ranging from about 1 μm to 1 cm. The degree of interaction between the colliding particles and the fluid in which they are suspended can be characterized by a dimensionless parameter called the Stokes number, St, which is defined as the ratio of the characteristic time scale τ_p for particle drift relative to the fluid and the fluid time scale τ_f. For sufficiently small particles the Stokes drag law can be used to write the particle time scale as $\tau_p = m/3\pi\mu d$, where *m* and *d* are the particle mass and diameter, respectively, and μ is the fluid viscosity. The fluid time scale is typically taken to be the fluid convective time, given by the ratio $\tau_f = L/U$ of the characteristic fluid length scale *L* to the fluid velocity scale *U*. The current paper examines the influence of fluid turbulence on contact electrification of colliding identical particles for different values of the particle Stokes number.

II. Computational Method

A. Particle Transport

The particle collisions were simulated using the hard-sphere model, as described by Crowe et al. [33]. The hard-sphere model solves the particle impulse equations during collisions to obtain the post-collision particle velocities $\mathbf{v}_n(i+1)$ from the given pre-collision velocities $\mathbf{v}_n(i)$ and restitution coefficient e. For two particles labeled 1 and 2, the restitution coefficient is defined by

$$e_{rest} \equiv \frac{\left|\mathbf{v}_1(i+1) - \mathbf{v}_2(i+1)\right|}{\left|\mathbf{v}_1(i) - \mathbf{v}_2(i)\right|}, \tag{1}$$

where **n** is the unit normal vector from the centroid of particle 1 to that of particle 2. The hard-sphere model also solves the angular impulse equations to obtain the particle angular rotation rate after the collision. The model uses Coulomb's law of friction for the sliding force and assumes that once a particle stops sliding, there is no later sliding of the particle. During the time period in-between collisions, the simulation method solves the particle momentum and angular momentum equations for the particle velocity and rotation rate, subject to forces and torques induced by the fluid, including viscous drag and torque, Saffman lift [34-35], and Magnus lift [36]. Added mass force, pressure gradient force and Bassett force are negligible based on the parameter values used in the computations. Electrostatic forces (Coulomb and dielectrophoretic forces) were also neglected on the assumption that particle charges were too weak for these forces to be significant in comparison to the fluid drag. The fluid velocity was interpolated from a 128^3 Cartesian grid onto the particle locations with cubic accuracy using the $\mathrm{M}4'$ variation of the B-spline interpolation method developed by Monaghan [37].

As two particles collide, the contact force between the particles is transmitted via a flattened contact region, across which the particle surfaces are separated by a small gap of width δ. The gap thickness is on the order of a nanometer, which for micrometer-scale or larger particles is much less than the particle diameter. For spherical particles, the contact region has a circular shape with radius $a(t)$. For non-adhesive particles, the contact region radius starts at a value of zero at the onset of contact, increases during the compression stage of the collision to a maximum value of $a_{\max}$, and then decreases again during the recovery stage of the collision until it vanishes again at the particle detachment point. An expression for the maximum contact region radius can be obtained using the Hertz [38] contact theory as

$$a_{\max} = \left(\frac{15 M w_r^2 R^2}{16 E}\right)^{1/5}, \tag{2}$$

where $w_r = \left|[\mathbf{v}_2(i) - \mathbf{v}_1(i)] \cdot \mathbf{n}\right|$ is the relative radial velocity between two particles labeled '1' and '2' prior to the i^{th} collision, and M, R and E are the effective mass, radius and elastic coefficient of the colliding particle pair, defined by

$$\frac{1}{M} \equiv \frac{1}{m_1} + \frac{1}{m_2}, \qquad \frac{1}{R} \equiv \frac{1}{r_1} + \frac{1}{r_2}, \qquad \frac{1}{E} \equiv \frac{1-\nu_1^2}{E_1} + \frac{1-\nu_2^2}{E_2}. \tag{3}$$

Here m_n, r_n, E_n, and ν_n denote the mass, radius, elastic modulus and Poisson's ratio for particle n, respectively.

B. Contact Electrification

The phenomenological contact electrification model used in the current study is a stochastic version of the model proposed by Duff and Lacks [30] and Lacks and Levandovsky [28]. The original model assumed that the charge carrier for contact electrification is a set of electrons trapped in high-energy band gaps, which transfer into a low-energy state when transported to a second particle during particle collision. However, it was noted by Castle [39] that the model is equally valid with ions as the charge carrier (see also [21]). The number of charge carriers at time *t* is denoted by $N_{H,n}(t)$ on a particle *n* with diameter d_n. If the initial surface number density of charge carriers is ρ_n, then $N_{H,n}(0) = \pi d_n^2 \rho_n$. When a particle collides with another particle, each particle transfers to the other particle all of the charge carriers within a distance r_{cut} of the contact point, where the contact point is the centroid of the contact region. For instance, in a collision between particles 1 and 2 at a time t_c in which charge carriers are exchanged between both particles, the change in number of charge carriers, $N_{H,n}(t)$, for each particle is given by

$$\Delta N_{H,1} = -\pi r_{cut}^2 \rho_1 , \qquad \Delta N_{H,2} = -\pi r_{cut}^2 \rho_2 . \tag{4}$$

The change in particle charge due to the collision is given simply by the product of the number of charge carriers exchanged and the electric charge e_C per charge carrier. Duff and Lacks [30] examined several different values for the distance r_{cut} and found that the value selected did not significantly modify the qualitative nature of the contact electrification predictions. Since typical charge carriers, such as high-energy electrons or ions, can only travel short distances either between particles or on a particle surface, the physically correct value of r_{cut} is the maximum contact region radius $a_{\max}$, given by (2). However, this choice can lead to a requirement for a large number of computations per particle in order to observe significant contact electrification, and so might not be computationally feasible. A reasonable approach to accelerate the numerical computation is to prescribe r_{cut} to a be a multiple of $a_{\max}$, such that

$$r_{cut} = D a_{\max} , \tag{5}$$

where $D \geq 1$ is an acceleration factor.

At any time *t*, the surface of a particle consists of some regions with available charge carriers and some regions in which the charge carriers have already been cleared away by transfer to another particle. If particle 1 collides with a second particle 2 in a contact region with available charge carriers on particle 1 but without available charge carriers on particle 2, then the electric charge is transferred only from particle 1 to particle 2, but not from particle 2 to particle 1. Duff and Lacks [30] presented a computational approach in which they used a set of sub-particles attached to the particle surfaces to represent high-energy electrons on the surface, which were then removed within a region of radius r_{cut}

following each collision. Of course, this approach is quite time-consuming for large numbers of particles. In the current paper, we alternatively propose a stochastic approach for dealing with depletion of charge carriers from the particle surface. Specifically, we denote by $A_{H,n}(t)$ the total area on a particle *n* with available charge carriers at time *t*, such that at the initial time $A_{H,n}(0) = A_n \equiv \pi d_n^2$, where A_n is the surface area of particle *n*. A collision of particle 1 with another particle 2 is considered to consist of two stages – a *forward transfer* of charge carriers from particle 1 to particle 2 and a *reverse transfer* from particle 2 to particle 1. In the forward transfer stage, we select a random variable p_1 with uniform probability distribution between 0 and 1. If $p_1 \le A_{H,1}(t)/A_1$, then the collision is taken to have occurred at a location with available charge carriers on particle 1. In this case, the change in number of charge carriers and the change in area occupied by available charge carriers on particle 1 are given by

$$\Delta N_{H,1} = -\pi r_{cut}^2 \rho_1 , \qquad \Delta A_{H,1} = -\pi r_{cut}^2 . \tag{6}$$

If $p_1 > A_{H,1}(t)/A_1$, then the collision is taken to have occurred at a location with no available charge carriers on particle 1, and there is no change in the number of charge carriers or in $A_{H,1}$. In the reverse transfer stage, we again select a random number p_2 with the same probability distribution. If $p_2 \le A_{H,2}(t)/A_2$, then the collision is taken to have occurred at a location with available charge carriers on particle 2, such that

$$\Delta N_{H,2} = -\pi r_{cut}^2 \rho_2 , \qquad \Delta A_{H,2} = -\pi r_{cut}^2 . \tag{7}$$

Again, no changes are made if $p_2 > A_{H,2}(t)/A_2$. After both the forward and reverse transfer stages of contact electrification are completed, the net change in charge of the two particles over the time step is given by

$$\Delta Q_1 = -\Delta Q_2 = e_C (\Delta N_{H,1} - \Delta N_{H,2}) . \tag{8}$$

C. Fluid Flow

Isotropic, homogeneous turbulence was numerical generated using the pseudo-spectral direct numerical simulation (DNS) approach of Vincent and Meneguzzi [40]. In this approach, the computational domain is a triply-periodic cube, and we use second-order Adams-Bashforth time stepping for the nonlinear convection term and exact integration for the viscous term. The spectral Navier-Stokes equations were evolved in time after having been projected onto a divergence-free space using the operator $P_{ij} = k_i k_j / k^2 - \delta_{ij}$ according to the expression

$$\begin{aligned}\overline{\mathbf{u}}^{n+1} &= \overline{\mathbf{u}}^{n} \exp(-\nu\, k^2 \Delta t) \\ &\quad + \Delta t\ \mathbf{P}\cdot\left[\frac{3}{2}\overline{\mathbf{F}}^{n} \exp(-\nu\, k^2 \Delta t) - \frac{1}{2}\overline{\mathbf{F}}^{n-1} \exp(-2\nu\, k^2 \Delta t)\right]\end{aligned} \tag{9}$$

where an overbar denotes Fourier transform in three space dimensions, a superscript indicates the time step, and **k** is the wavenumber vector with magnitude *k*. The Fourier transform of the force vector **F** on the right-hand side of (9) is given by

$$\overline{\mathbf{F}} = \overline{\mathbf{u}\times\boldsymbol{\omega}} + \overline{\mathbf{f}}_F\,, \tag{10}$$

where $\overline{\mathbf{f}}_F$ is the small wavenumber forcing term required to maintain the turbulence with approximately constant kinetic energy. The velocity field was made divergence-free at each time step by taking its Fourier transform and using the spectral form of the continuity equation, given by

$$\mathbf{k}\cdot\overline{\mathbf{u}} = 0\,. \tag{11}$$

The forcing vector was assumed to be proportional to the fluid velocity [41-42], such that

$$\overline{\mathbf{f}}_F = \begin{cases} C\overline{\mathbf{u}} & \text{for } k < k_{crit} \\ 0 & \text{for } k > k_{crit} \end{cases}, \tag{12}$$

where the coefficient *C* was adjusted at each time step in order to maintain constant turbulent kinetic energy (in spectral space). The current computations were performed with $k_{crit} = 5$, so that the forcing acts only on the large-scale eddies.

The fluid flow computations were performed on a 128^3 cubic grid with domain side length 2π. A preliminary computation was conducted with no particles to allow the turbulence to develop a range of length scales characteristic of statistically stationary homogeneous isotropic turbulence for 5000 time steps with a time step size of $\Delta t = 0.005$. The computation was then restarted with 64,000 particles randomly distributed in the computational domain and with the initial particle velocity set equal to the local fluid velocity. The turbulence kinetic energy *q* and dissipation rate ε were obtained from the power spectrum, $E(k)$, as

$$q = \int_0^{k_{\max}} E(k)dk\,, \qquad \varepsilon = 2\nu\int_0^{k_{\max}} k^2 E(k)dk\,. \tag{13}$$

Various dimensionless measures describing the turbulence in the validation computations are listed in Table 1, including the root-mean-square velocity magnitude u_0, the average turbulence kinetic energy *q*, the integral length scale $\ell_0 = 0.5\, u_0^{\,3}/\varepsilon$, the Taylor micro-

scale $\lambda = (15\nu/\varepsilon)^{1/2} u_0$, and the Kolmogorov length scale $\eta = (\nu^3/\varepsilon)^{1/4}$. The corresponding microscale Reynolds number is $\mathrm{Re}_\lambda = u_0\lambda/\nu = 99$.

TABLE 1. DIMENSIONLESS SIMULATION PARAMETERS AND PHYSICAL PARAMETERS OF THE FLUID TURBULENCE.

Simulation Parameters		**Turbulence Parameters**	
Time step	0.005	Turbulent kinetic energy, q	0.115
Cycles	50000	Dissipation rate, ε	0.009
Grid	128^3	Kinematic viscosity, ν	0.001
		Integral length, ℓ_0	1.18
		Taylor microscale, λ	0.357
		Kolmogorov length, η	0.0183
		Integral velocity, u_0	0.277
		Integral time, T_ℓ	4.26

III. RESULTS AND DISCUSSION

A. Characteristics of the Fluid Flow

The direct numerical simulations (DNS) of the turbulent flow field were conducted assuming one-way coupling with the particles. The computed power spectrum $e(k)$ is plotted in Fig. 1a as a function of the product of the wavenumber magnitude *k* and the Kolmogorov length scale $\eta = (\nu^3/\varepsilon)^{1/4}$, showing the expected $k^{-5/3}$ dependence in the inertial range and a faster drop-off for higher wavenumber in the dissipation range. The computed velocity probability density function (p.d.f.) in one coordinate direction (*x*-direction), normalized by the root-mean-square velocity, is shown in Fig. 1b. The DNS predictions are observed to be close to a best-fit Gaussian curve $p(v) = 0.8\exp(-0.5v^2)$, where $v \equiv v_x / v_{x,rms}$, in agreement with standard observations for the turbulence flows [43]. The p.d.f. of the *x*-component of the fluctuating fluid acceleration field is plotted in Fig. 1c. Fluid acceleration is computed from the DNS velocity field for post-processing purposes using a centered difference approximation in space and a forward difference in time. Also shown in this fig. is the empirical expression for the p.d.f.,

$$p(a) = 1.8\exp\left[-a^2/\{(1+|ac_1/c_2|^{c_3})c_2^2\}\right], \qquad (14)$$

obtained experimentally by La Porta et al. [44]. In this expression, $a \equiv a_x / a_{x,rms}$, and the coefficients are given by a best fit to La Porta et al.'s experimental data as $c_1 = 0.539$,

$c_2 = 0.508$, and $c_3 = 1.588$. The acceleration p.d.f. exhibits a non-Gaussian "superstatistical" distribution characterized by a fat tail, which is typical of a highly intermittent signal [45-47]. Mordant et al. [48] suggested that the observed acceleration intermittency in turbulent flows can be associated with the presence of coherent vortex structures.

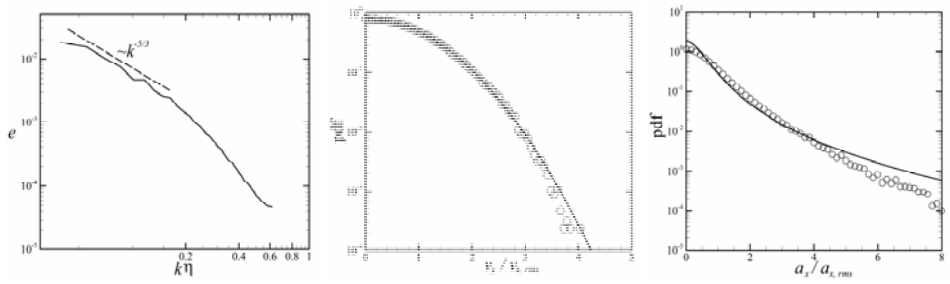

(a) (b) (c)

Fig. 1. Plots characterizing direct numerical simulations of turbulent flow: (a) power spectrum showing $k^{-5/3}$ scaling in inertial range, (b) velocity probability density function with DNS data (symbols) and best-fit Gaussian curve (solid line), and (c) probability density function for acceleration with DNS data (symbols) and best-fit function to the experimental data of La Porta et al. [44] (solid line).

B. Effect of Stokes Number on Contact Electrification

The effect of fluid flow on the particle collision and electrification was examined by conducting a series of simulations with different values of the Kolmogorov-scale Stokes number, St, defined by

$$\mathrm{St} = \frac{\tau_P}{\tau_K} . \tag{15}$$

Here, the particle time scale $\tau_P = m / 3\pi d\mu$ is a function of the particle mass m and diameter d and the fluid viscosity μ, and the Kolmogorov time scale is defined by $\tau_K = (\nu / \varepsilon)^{1/2}$. Computations were performed for a set of six Stokes numbers ranging from 1.1 to 33.6. In all computations, the total number collisions in the system $B(t)$ exhibits approximately linear increase with time after a short transient period. The slope of $B(t)$ following the initial transient, divided by the computational volume $(2\pi)^3$, yields the collision rate per unit volume, $\dot{n}_c$. We plot the variation of $\dot{n}_c$ with the Stokes number in Fig. 2. The collision rate exhibits a peak near $\mathrm{St} = 5$.

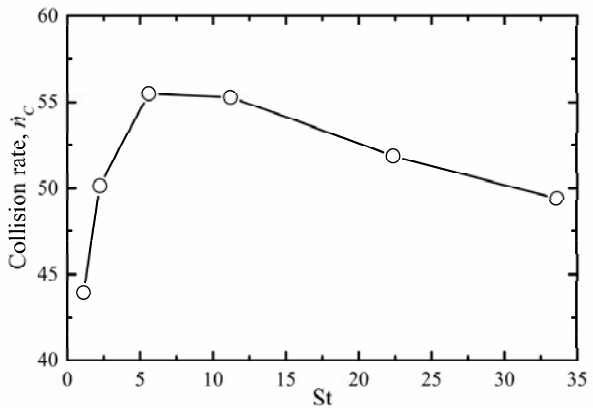

Fig. 2. The collision rate per unit volume, $\dot{n}_c$, for different values of the Kolmogorov-scale Stokes number St.

The approach of the particle system to an equilibrium charge state can be observed by plotting the time variation of the total transferred charge, Q_{trans}, defined as half of the sum of the absolute value of the charge of each particle. The total transferred charge is plotted in Fig. 3 as a function of time for different Stokes numbers. The value of Q_{trans} approaches an equilibrium value at long time, after all the charge carriers initially attached to the particles in the system have been expended via collisions with other particles in the system. The larger the collision rate $\dot{n}_c$, the more opportunities for a particle to transfer charge, and hence the more quickly this equilibrium condition is attained. However, the results in Fig. 3 also depend on the relative velocity at collision between the particles, which effects the contact area as indicated in (2) and hence the number of charge carriers that are transferred at each collision. For Stokes numbers above about 6, the differences in value of $\dot{n}_c$ in Fig. 2 and in the plot of Q_{trans} versus time in Fig. 3 are observed to be small.

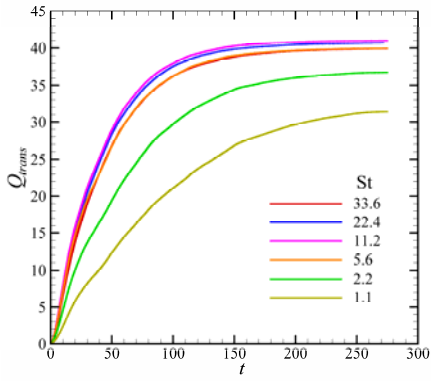

Fig. 3. The time development of total transferred charge Q_{trans} for different Stokes numbers.

For a closer examination of particle collision, we count the number of collisions for each particle, denoted by b_p, and compute the probability density function (p.d.f.) of collision number by dividing the range of variation of b_p into equal-size bins. The resulting p.d.f. for collision number is plotted in Fig. 4 for St = 33.6 at five different values of the total number of collisions in the system, *B*. The p.d.f. of collision number at this Stokes number is observed to closely approximate a normal distribution, as indicated by the curves plotted in Fig. 4. As run time increases and the total number of collisions in the system accumulates, the distribution of number of collisions grows wider. To facilitate a comparison of different Stokes number cases, the collision number p.d.f. is plotted in Fig. 5 by dividing the value of b_p by the total number of collisions B, and also by multiplying the value of the *y*-axis variable by *B* to ensure that the integral of the p.d.f. is equal to unity. The plot in Fig. 5 is made for different Stokes number values at a time when the total number of collisions is $B = 500{,}000$. The resulting p.d.f. plot approaches a common normal distribution as the value of Stokes number increases, with mean value $\langle b_p / B \rangle = 3.1 \times 10^{-5}$.

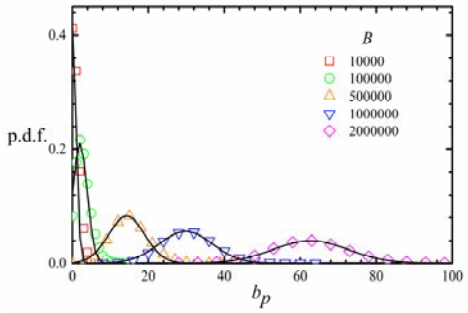

Fig. 4. The probability density function (p.d.f.) of the number of collisions for a particle, b_p, for a case with St = 33.6, plotted at different values of the total number of collisions in the system, *B*. The black solid lines represent best-fit normal distributions.

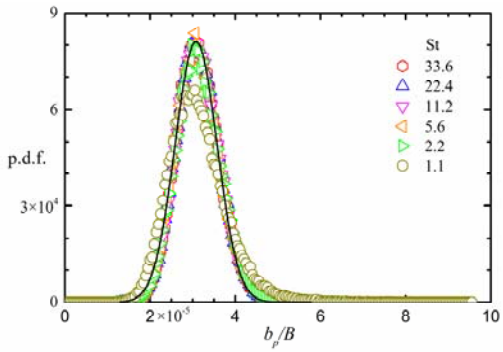

Fig. 5. The probability density function (p.d.f.) of nondimensionless collision number of particle, b_p/B, for different Stokes numbers when the total number of collisions $B = 500{,}000$. The black solid line represents the best-fit normal distribution in the high-St limit.

The observation that the collision distribution approaches a normally-distributed p.d.f. can be explained with use of the central limit theorem. For each collision, the probability that a given particle *i* is involved in this collision is

$$p = \frac{N_p - 1}{N_p(N_p - 1)/2} = \frac{2}{N_p}, \tag{16}$$

where N_p is the total number of particles in the computational system. Assuming linear variation in time *t*, the total number of collisions *B* can be written as $B = \dot{n}_c V t$, where *V* is the volume of the computational domain. After *B* collisions in the system, the probability of particle *i* having undergone *s* collisions can be expressed as

$$P(s,B) = \binom{B}{s} p^s (1-p)^{B-s}, \tag{17}$$

which is a binomial distribution with mean $\mu = Bp$ and variance $\sigma^2 = Bp(1-p)$, where p is a constant given by (16). When *B* becomes large, Stirling's approximation $B! \sim B^B e^{-B}\sqrt{2\pi B}$ can be used to yield an asymptotic approximation for (17) as

$$P(s,B) \sim (\frac{Bp}{s})^s (\frac{B(1-p)}{B-s})^{B-s} \sqrt{\frac{B}{2\pi s(B-s)}}. \tag{18}$$

Under the further assumption that $\left|\frac{s}{pB} - 1\right| << 1$, the term $(\frac{Bp}{s})^s (\frac{B(1-p)}{B-s})^{B-s}$ in (18) can be approximated as $e^{-(s-Bp)^2/2Bp(1-p)}$ with use of the Taylor series expansion for $\ln(1+x) = x - \frac{1}{2}x^2 + \mathrm{O}(x^3)$, so that (18) becomes

$$P(s,B) \sim \sqrt{\frac{1}{2\pi Bp(1-p)}} e^{-(s-Bp)^2/2Bp(1-p)} = \frac{1}{\sqrt{2\pi\sigma^2}} e^{-\frac{(s-\mu)^2}{2\sigma^2}}. \tag{19}$$

The asymptotic approximation (19) for $P(s,B)$ is a normal distribution with mean μ and variance σ^2. Since the particles are identical and independent, $P(s,B)$ also represents the probability distribution of collision number for the particles. We note that the assumption that the particle collisions are independent holds only for large Stoke numbers. For small St, two particles that have recently collided would be more likely to collide with each other again, so that the collisions would no longer be independent.

The probability distribution function of the radial relative velocity (RRV) at contact is shown for different Stokes numbers in Fig. 6. For large Stokes numbers (St > 10), the RRV distribution is found to be closely fit by the skew-normal distribution, $y = \frac{5}{\sqrt{2\pi}} e^{-\frac{1}{2}(\frac{x-0.05}{0.2})^2} [1 + \mathrm{erf}(\frac{24(x-0.05)}{\sqrt{2}})]$, where erf($x$) is the error function. For smaller values of the Stokes numbers (e.g., St = 1.1), the RRV distribution is close to the exponential distribution, $y = e^{2.4125-10.25x}$. As St decreases, the mean value of the RRV distribution also decreases, implying small contact area and small amounts of charge transfer during collisions.

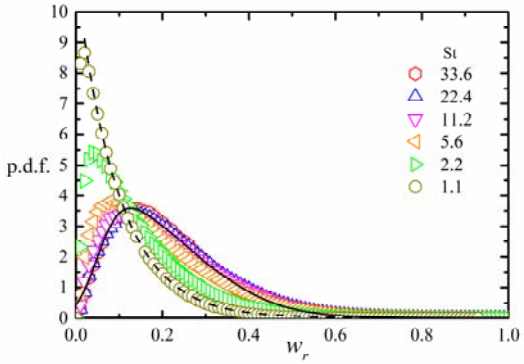

Fig. 6. The probability density function (p.d.f.) of radial relative velocity at contact, w_r, for different Stokes numbers when B=500,000. The solid line is a skew-normal distribution, and the dashed line is an exponential distribution.

In these computations, it was assumed that each particle is initially completely covered by available charge carriers, which the particles gradually lose by collisions with other particles until no available charge carriers remain. We define a particle as being 'involved in the electrification processes' if it has undergone at least one collision but still has some available charge carriers remaining. The ratio of available charge carriers at the current time to that at the start of the computation is called the *charge carrier depletion ratio*, $R_{H,n}(t)$, which is defined for particle *n* by

$$R_{H,n}(t) = \frac{N_{H,n}(t)}{N_{H,n}(0)}, \tag{20}$$

where $N_{H,n}(0)$ and $N_{H,n}(t)$ are the number of available charge carriers of particle *n* at the initial time and at time *t*, respectively. The charge carrier depletion ratio $R_{H,n}(t)$ is equal to unity at the start of the computation for all particles, and it approaches zero at long time as all available charge carriers are expended by transferring onto colliding particles. Fig. 7 shows the time development of the distribution of $R_{H,n}(t)$ for all particles involved in the electrification process for different values of the total number of colli-

sions *B*, for a case with St = 33.6. As the total collision number *B* increases, the peak of distribution moves from nearly unity to nearly zero.

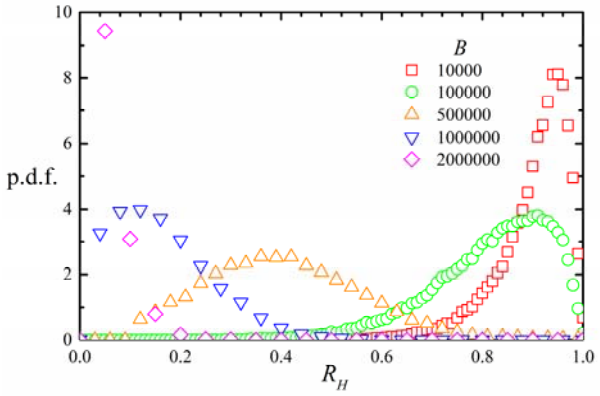

Fig. 7. Time variation of the p.d.f. of the charge carrier depletion ratio $R_{H,n}(t)$ for particles involved in the electrification process for a case with St = 33.6, plotted at different values of the total number of collisions *B*.

A plot showing the p.d.f. of the charge carrier depletion ratio for different Stokes numbers when $B = 500{,}000$ is given in Fig. 8. At this intermediate stage, most of the particles are involved in the electrification process and the p.d.f. is observed to be close to a normal distribution. The mean value of the $R_{H,n}(t)$ distribution represents the average ratio of charge carriers that have been expended at a given time. The distributions of $R_{H,n}(t)$ are almost the same for cases with different Stokes numbers for large values of St, while the mean value of $R_{H,n}(t)$ is larger for small St values. The p.d.f. distribution for $R_{H,n}(t)$ at the midpoint of the electrification process, when the mean value $\langle R_{H,n} \rangle \cong 0.5$, is plotted in Fig. 9 for different Stokes numbers. We similarly see that the normal distribution is a good fit for all cases, but that the variance of the distribution is somewhat smaller at small St than at large St values, which is related to the observed lower values of the relative radial velocity for small Stokes numbers.

The net charge on each particle is zero at the beginning of the computation. Charge is exchanged between the particles during the contact electrification process until the equilibrium state is reached, at which time all of the available charge carriers have been expended and after which the charge on each particle remains constant. A plot of the distribution of particle charge, q_p, in the equilibrium state is given in Fig. 10. The equilibrium charge distribution is observed to form a nearly normal distribution which has somewhat smaller variance for small Stokes numbers, but to asymptote to a common curve for large Stokes numbers.

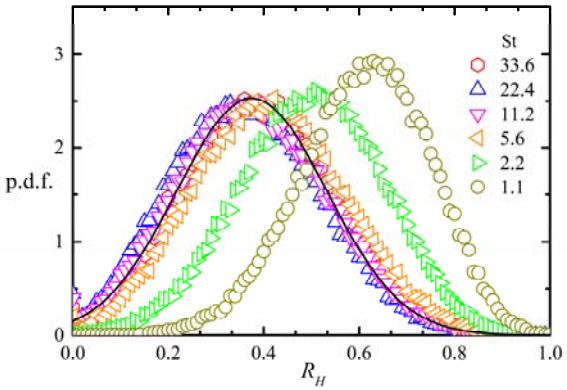

Fig. 8. The probability density function (p.d.f.) of the charge carrier depletion ratio R_H for different Stokes numbers when the total number of collisions $B=500{,}000$. The solid line denotes the best-fit normal distribution to the high St cases.

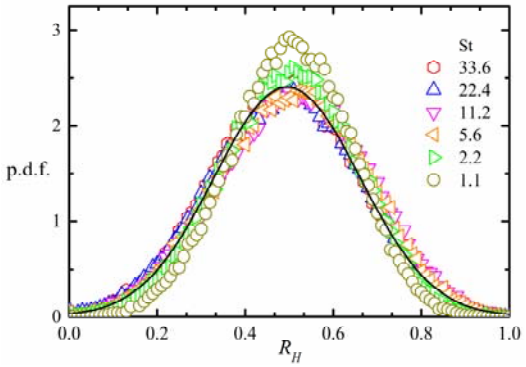

Fig. 9. The distribution of R_H for different Stokes numbers when the mean value $\langle R_{H,n} \rangle \approx 0.5$. The solid line is the best-fit Gaussian to the high St cases.

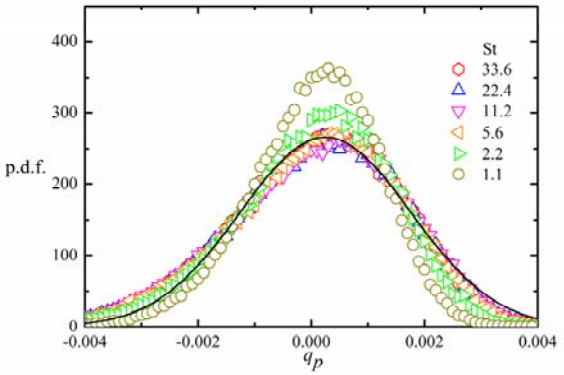

Fig. 10. The distribution of charge of particle q_p for different Stokes numbers when $B=2{,}000{,}000$. The solid line is the best-fit Gaussian curve to the high St cases.

IV. Conclusion

We have coupled a probabilistic version of a phenomenological contact electrification model to a pseudo-spectral direct numerical simulation method for homogeneous turbulence and a hard-sphere discrete-element method for particle transport and collisions in order to advance understanding of the effect of fluid turbulence on particle contact electrification. The observed distributions of particle charge development are found to be insensitive to Stokes number for St greater than about 6, but to be highly sensitive to Stokes number for values of St near unity.

The probability density functions for number of collisions and for number of charge carriers are observed to be approximately normally distributed for high St cases, as would be expected from the central limit theorem for independent random processes. However, for small St cases (near unity and below), the particle relative radial velocity at collision is observed to approach an exponential distribution, indicating an increased tendency for collision between neighboring particles, which leads to a break-down of the assumption of independent collisions. The particle charge approaches a constant value at large time, when all of the available charge carriers have been removed from the particle surfaces via collisions. The resulting charge distribution is found to be well approximated by a normal distribution for all Stokes number values examined. Cases with high Stokes number (above about 6) approach an asymptotic charge distribution which is nearly independent of Stokes number. Cases with lower Stokes number values, near unity, also seem to approach a nearly normal charge distribution, but with significantly smaller variance than for the high Stokes number cases.

References

[1] J. S. Marshall, and S. Q. Li, *Adhesive Particle Flow: A Discrete Element Approach*. New York, NY: Cambridge University Press, 2014.

[2] R. K. Eckhoff, *Dust Explosions in the Process Industries*, 2nd ed. Oxford, UK: Butterworth-Heinemann, 1997.

[3] J. Latham, "The electrification of snowstorms and sandstorms," *Quart. J. Roy. Meteorol. Soc.*, vol. 90, pp. 91-95, Jan. 1964.

[4] E. Williams, N. Nathou, E. Hicks, C. Pontikis, B. Russell, M. Miller and M. J. Bartholomew, "The electrification of dust-lofting gust fronts ('haboobs') in the Sahel,", *Atmos. Res* , vol. 91, pp. 292-298, Feb. 2009.

[5] X. J. Zheng, "Electrification of wind-blown sand: Recent advances and key issues," *Eur. Phys. J. E,* vol. 36, no. 12, p.138, Dec 2013.

[6] M. Brook, C. B. Moore, and T. Sigurgeirsson, "Lightning in volcanic clouds," *J. Geophys. Res.,* vol. 79, no. 3, pp. 472-475, Jan. 1974.

[7] R. J. Thomas *et al.*, "Electrical activity during the 2006 Mount St. Augustine volcanic eruptions," *Science,* vol. 315, no. 5815, pp. 1097-1097, Feb. 2007.

[8] H. F. Eden and B. Vonnegut, "Electrical breakdown caused by dust motion in low-pressure atmospheres: Considerations for Mars," *Science*, vol. 180, no. 4089, pp. 962-963, Jun. 1973.

[9] K. M. Forward, D. J. Lacks, and R. M. Sankaran, "Particle-size dependent bipolar charging of Martian regolith simulant," *Geophys. Res. Lett.,* vol. 36, no. 13, p. L13201, Jul. 2009.

[10] R. G. Harrison *et al.*, "Applications of Electrified Dust and Dust Devil Electrodynamics to Martian Atmospheric Electricity," *Space Sci. Rev.,* vol. 203, no. 1, pp. 299-345, Apr. 2016.

[11] C. P. R. Saunders, "Thunderstorm Electrification Laboratory Experiments and Charging Mechanisms," *J. Geophys. Res.: Atmospheres,* vol. 99, no. D5, pp. 10773-10779, May. 1994.

[12] J. H. Helsdon, W. A. Wojcik, and R. D. Farley, "An examination of thunderstorm-charging mechanisms using a two-dimensional storm electrification model," *J. Geophys. Res.: Atmospheres,* vol. 106, no. D1, pp. 1165-1192, Jan. 2001.

[13] T. W. Hartquist, O. Havnes, and G. E. Morfill, "The effects of charged dust on Saturn's rings," *Astron. Geophys.,* vol. 44, no. 5, pp. 26-30, Oct. 2003.
[14] S. Kempf, U. Beckmann, R. Srama, M. Horanyi, S. Auer, and E. Grün, "The electrostatic potential of E ring particles," *Planet. Space Sci.,* vol. 54, no. 9–10, pp. 999-1006, Aug. 2006.
[15] S. J. Desch and J. N. Cuzzi, "The generation of lightning in the solar nebula," *Icarus,* vol. 143, no. 1, pp. 87-105, Jan. 2000.
[16] M. W. Williams, "Triboelectric charging of insulators - Mass transfer versus electrons/ions," *J. Electrostatics,* vol. 70, no. 2, pp. 233-234, Apr. 2012.
[17] H. T. Baytekin, B. Baytekin, J. T. Incorvati, and B. A. Grzybowski, "Material Transfer and Polarity Reversal in Contact Charging," *Angew. Chem. Int. Ed.,* vol. 51, no. 20, pp. 4843-4847, May. 2012.
[18] L. S. McCarty and G. M. Whitesides, "Electrostatic charging due to separation of ions at interfaces: Contact electrification of ionic electrets," *Angew. Chem. Int. Ed.,* vol. 47, no. 12, pp. 2188-2207, Feb. 2008.
[19] D. J. Lacks and R. M. Sankaran, "Contact electrification of insulating materials," *J. Phys. D: Appl. Phys.,* vol. 44, no. 45, p. 453001, Nov. 2011.
[20] S. R. Waitukaitis, V. Lee, J. M. Pierson, S. L. Forman, and H. M. Jaeger, "Size-Dependent Same-Material Tribocharging in Insulating Grains," *Phys. Rev. Lett.,* vol. 112, no. 21, pp. 218011, May. 2014.
[21] J. Lowell and A. C. Roseinnes, "Contact Electrification," *Adv. Phys.,* vol. 29, no. 6, pp. 947-1023, Jul. 1980.
[22] W. R. Harper, *Contact and Frictional Electrification*. New York, NY: Oxford University Press, 1967.
[23] S. Kittaka and Y. Murata, "Photoelectric Emission and Contact Charging of Vacuum-UV Irradiated Polymers," *Jpn. J. Appl. Phys.,* vol. 18, no. 3, pp. 515-521, Mar. 1979.
[24] J. Lowell and W. S. Truscott, "Triboelectrification of Identical Insulators .2. Theory and Further Experiments," *J. Phys. D: Appl. Phys.,* vol. 19, no. 7, pp. 1281-1298, Jul. 1986.
[25] J. F. Kok and D. J. Lacks, "Electrification of granular systems of identical insulators," *Phys. Rev. E,* vol. 79, no. 5, p. 051304, May 2009.
[26] T. Siu, J. Cotton, G. Mattson, and T. Shinbrot, "Self-sustaining charging of identical colliding particles," *Phys. Rev. E,* vol. 89, no. 5, p. 052208, May. 2014.
[27] H. T. Baytekin, A. Z. Patashinski, M. Branicki, B. Baytekin, S. Soh, and B. A. Grzybowski, "The Mosaic of Surface Charge in Contact Electrification," *Science,* vol. 333, no. 6040, pp. 308-312, Jul. 2011.
[28] D. J. Lacks and A. Levandovsky, "Effect of particle size distribution on the polarity of triboelectric charging in granular insulator systems," *J. Electrostatics,* vol. 65, no. 2, pp. 107-112, Feb. 2007.
[29] T. Pahtz, H. J. Herrmann, and T. Shinbrot, "Why do particle clouds generate electric charges?," *Nature Phys.,* vol. 6, no. 5, pp. 364-368, May. 2010.
[30] N. Duff and D. J. Lacks, "Particle dynamics simulations of triboelectric charging in granular insulator systems," *J. Electrostatics,* vol. 66, no. 1-2, pp. 51-57, Jan. 2008.
[31] L. Xie, G. Li, N. Bao, and J. Zhou, "Contact electrification by collision of homogenous particles," *J. Appl. Phys.,* vol. 113, no. 18, p.184908, May. 2013.
[32] M. M. Apodaca, P. J. Wesson, K. J. M. Bishop, M. A. Ratner, and B. A. Grzybowski, "Contact Electrification between Identical Materials," *Angew. Chem. Int. Ed.,* vol. 49, no. 5, pp. 946-949, Dec. 2010.
[33] C. T. Crowe, J. D. Schwarzkopf, M. Sommerfeld, Y. Tsuji, *Multiphase Flows with Droplets and Particles*, 2nd ed., Boca Raton, Florida: CRC Press, 2011.
[34] P. G. Saffman, "The lift on a small sphere in a slow shear flow," *J. Fluid Mech.,* vol. 22, no. 2, pp. 385-400, Jun. 1965.
[35] P. G. Saffman, "Corrigendum to 'The lift force on a small sphere in a slow shear flow'," *J. Fluid Mech., vol.* 31, pp. 624, Feb. 1968.
[36] S. I. Rubinow and J. B. Keller, "The transverse force on a spinning sphere moving in a viscous fluid," *J. Fluid Mech.,* vol. 11, no. 3, pp. 447-459, Nov. 1961.
[37] J. J. Monaghan, "Extrapolating B splines for interpolation," *J. Comput. Phys.,* vol. 60, no. 2, pp. 253-262, Sep. 1985.
[38] H. Hertz, "Über die Berührung fester elastischer Körper," *J. Reine Angew. Math.,* vol. 1882, no. 92, pp. 156-171, Jan. 1882
[39] G. S. P. Castle, "Contact charging between particles: some current understanding," in *Proceedings Electrostatics Society of America Annual Meeting*, Bloomington, MN, 2008, p. M1.
[40] A. Vincent and M. Meneguzzi, "The spatial structure and statistical properties of homogeneous turbulence," *J. Fluid Mech.,* vol. 225, pp. 1-20, 1991.

[41] T. S. Lundgren, “Linearly forced isotropic turbulence,” Annu. Research Briefs. CTR, Stanford, CA, Rep. 461-473, 2003.
[42] C. Rosales and C. Meneveau, "Linear forcing in numerical simulations of isotropic turbulence: Physical space implementations and convergence properties," *Phys. Fluids,* vol. 17, no. 9, p. 095106, Jul. 2005.
[43] G. A. Voth, K. Satyanarayan, and E. Bodenschatz, "Lagrangian acceleration measurements at large Reynolds numbers," *Phys. Fluids,* vol. 10, no. 9, pp. 2268-2280, May. 1998.
[44] A. La Porta, G. A. Voth, A. M. Crawford, J. Alexander, and E. Bodenschatz, "Fluid particle accelerations in fully developed turbulence," *Nature,* 10.1038/35059027 vol. 409, no. 6823, pp. 1017-1019, Feb. 2001.
[45] C. Beck, “Superstatistics: Theoretical concepts and physical applications,” in *Anomalous Transport: Foundations and Applications*, R. Klages, G. Radons and I. M. Sokolov, Ed. Weinheim, Germany: Wiley-VCH Verlag GmbH & Co. KGaA, 2008.
[46] L. Biferale, G. Boffetta, A. Celani, B. J. Devenish, A. Lanotte, and F. Toschi, "Multifractal Statistics of Lagrangian Velocity and Acceleration in Turbulence," *Phys. Rev. Lett.,* vol. 93, no. 6, p. 064502, Aug. 2004.
[47] A. M. Reynolds, "Superstatistical Mechanics of Tracer-Particle Motions in Turbulence," *Phys. Rev. Lett.,* vol. 91, no. 8, p. 084503, Aug. 2003.
[48] N. Mordant, E. Lévêque, and J. F. Pinton, “Experimental and numerical study of the Lagrangian dynamics of high Reynolds turbulence," *New J. Phys.,* vol. 6, no. 1, p. 116, Sep. 2004.